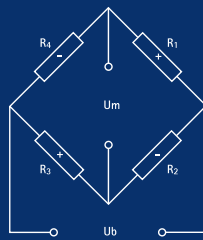


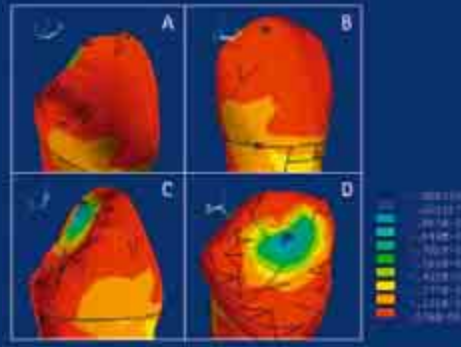
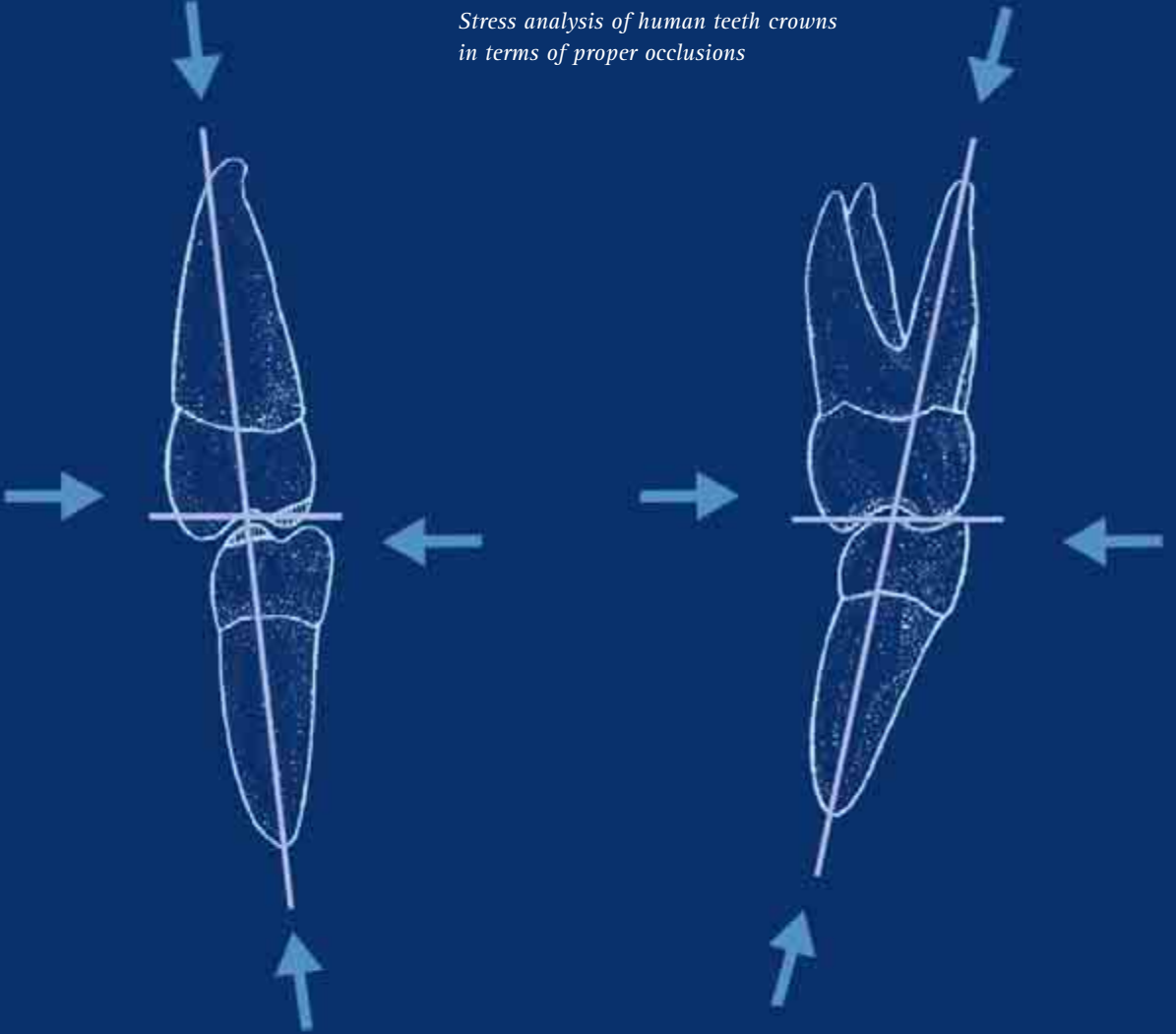
# reports in applied measurement



*Metrological analysis of stresses in a recycling machine for separating materials*



*Mechanical and thermal strain*



*Stress analysis of human teeth crowns in terms of proper occlusions*

# ram reports in applied measurement

## Metrological analysis of stresses in a recycling machine for separating materials

Mike Winkler, TU Chemnitz, Germany



Fig. 1: Recycling machine for separating compounds; on the right, the test version

### Preliminary remarks

Because of the constantly increasing pressure on our environment caused by solid waste and contaminants and the associated negative effect on our living conditions, the problems of technical pollution control are becoming ever more important. It is clearly a matter of urgent necessity to develop ecological as well as economically sensible recycling concepts.

More than enough reference documentation is available for existing disintegrator units such as shredders, ball mills, hammer mills, impact crushers, percussion grinders, granulators, rasps and screw crushers.

In contrast to this, there is currently hardly any scientifically based knowledge on the latest units to be used, which break down the compounds with flexible flaps moved by centrifugal force. So under a collaborative project involving Umwelt+Technik Chemnitz GmbH plant engineering and the Chair of Design Theory at the University of Technology TU Chemnitz, theoretical and experimental investigations were carried out on a new type of recycling machine for separating compounds (Fig. 1).

The main advantages of the machine under investigation here lie in the simple, economical disintegrator tool and the more effective

use of energy. For use in electronic scrap recycling, there is an additional advantage, as the process determines that a better method of disintegration is used, where less than 15% of the electronic components are destroyed.

In order to investigate the design of the actuator of the recycling machine and optimize pulverization of the material, it had to be possible to record, both visually and metrologically, the behavior of the machine when pulverizing the different materials and compounds.

*Figs. 2a, 2b:  
Recycling machine without  
the drive (CAD drawing)*



### Construction and function of the recycling machine

Figures 2a and 2b show the recycling machine as a three-dimensional CAD drawing. As can be seen in these drawings, the cylindrical container holds a rotor, to which independently movable chains are attached. These chains act as the impact tool for disintegration. The material disintegrates as it is intermittently subjected to impact stress, rebound stress and shearing stress. The rotor is driven by an electric motor ( $P = 132 \text{ kW}$ ) via a belt drive (not shown). The speed of the rotor is  $n = 750 \text{ rpm}$ .

The aim of these experimental investigations was to analyze the pulverization behavior of different homogeneous materials and compound products and to develop a model of the predicted process. Figure 3 shows some typical materials and compounds both before and after disintegration.

A high-speed camera was used to visually record pulverization for process analysis. Individual images from this film sequence are shown in Figures 13 and 14 (page 7). Basically, this was used to investigate the behavior of the materials during disintegration. It was also possible to clarify the impact and acceleration behavior of the chains.

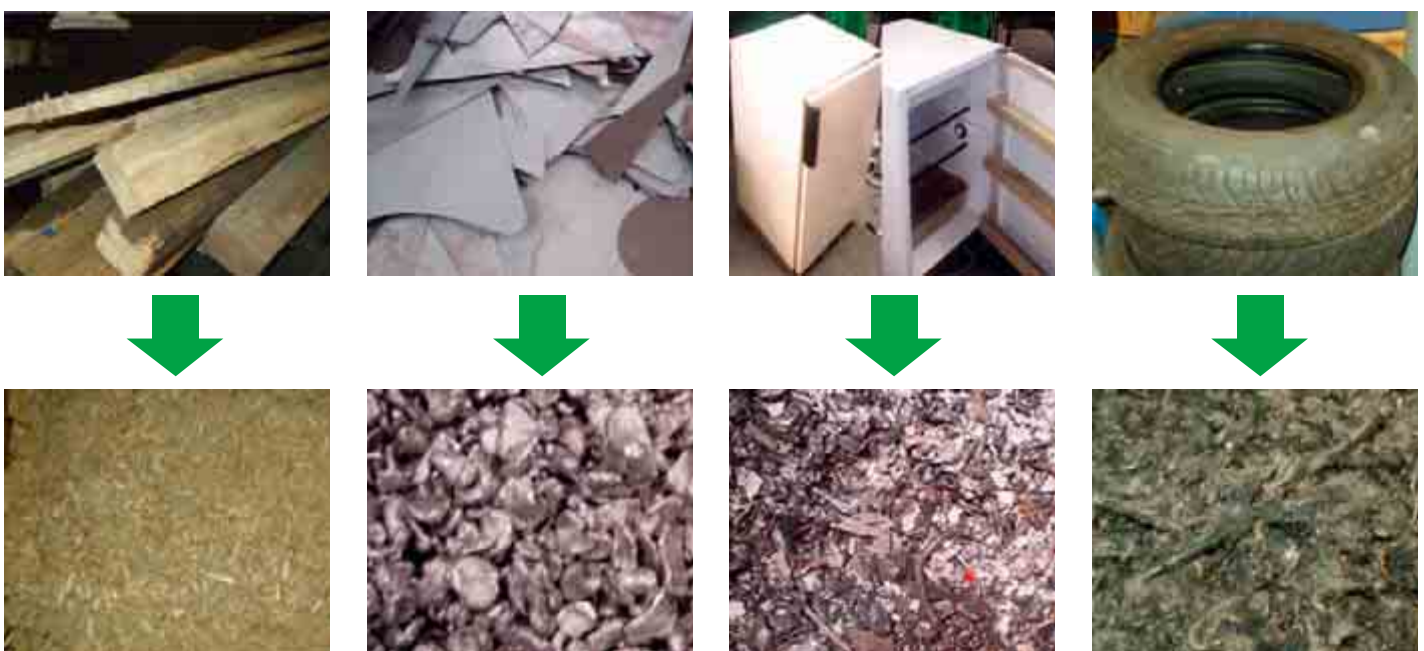


*Fig. 3: Materials and compounds under investigation (wood up to 100 x 100 mm, steel plate up to 0.6 mm, refrigerators, tires)*

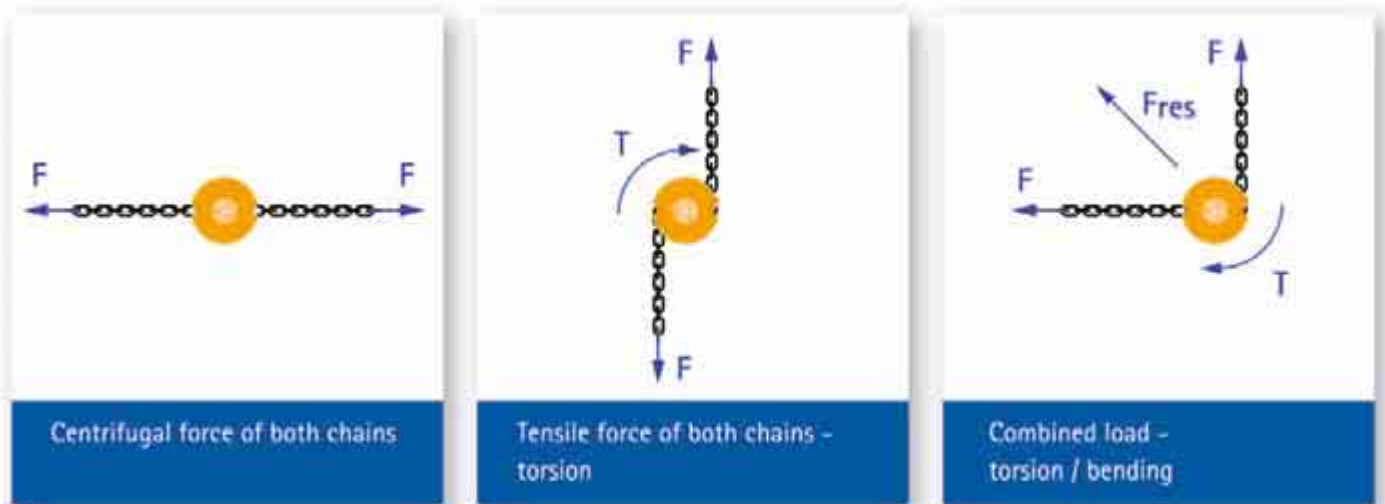


Fig. 4: Basic stresses during material pulverization

### Metrological analysis

Metrological analysis of the mechanical stresses was also necessary, in order to define the loading of the different components during the disintegration process and thus to provide a scientific basis for the dimensioning of the machine and the drive. Figure 4 shows in diagrammatic form the basic loads to be expected during operation. These are the tensile forces in the chains, the torsional moment in the input shaft and the resultant bending moment, also in the input shaft.

### The measurement task ...

... was to continuously record these quantities while the machine was in operation, in the different phases of material disintegration. It should be taken into consideration that during operation, the disintegration process pro-

duces changes in the measured quantities with a very high frequency. Furthermore, all the operating conditions are very rough and the temperature increases greatly during measurement.

### Metrology

To measure the load on the input shaft of the rotor (Fig. 5), it was equipped with an SG full bridge for torsion and with two SG half bridges mutually offset by 90° to record bending.

An area on the shaft between the bearing points, where the maximum bending moment is calculated to be, was found for installing the strain gages. HBM's 6/120LY11 strain gages were installed on the shaft to determine the bending stress. Geometrically, they are aligned

a defined distance away from the shoulder of the shaft, on the chain attachment plane or offset by 90°. Each of the two strain gages associated with a plane were connected to a half bridge, with both SGs active. The torsional stress is detected on the basis of strains recorded by HBM's type 3/120XY21 torsion strain gages. Two pairs of the type mentioned are connected to a full bridge with four active SGs. The cold-setting adhesive X280 was used for installation. The measuring points were first covered with PU 120 polyurethane paint and allowed to dry before being given extra protection against external influences by flexible, self-adhesive tape. Holes were made for the wiring to the preamplifiers and the slipping transformer located inside the shaft and at the end of the shaft.



Fig. 5: SG installation and wiring on the input shaft, SG full bridge (torsion), 2 SG half bridges (bending on two axes)



Fig. 6: Chain support, welded version

These are already marked in Figure 5. During operation, the temperature in this area of the shaft rises to about 80 °C. But by using SGs adapted to the shaft material and by connecting to half and full bridges, it was possible to reduce the effect of thermal expansion and obtain stable measurement results, whatever the temperature.

### Measurement of the tensile force of the chains ...

... was particularly difficult, because of the extremely rough ambient conditions existing inside the recycling machine. So it was not possible to install the strain gages in the interior, for example on the first link of the chain or to mount a force transducer on the chain support system, as during the disintegration process, the whole of the interior is exposed to the effect of the granular particles moving at high speed and any components not heavily protected would be destroyed in no time at all. The original welded chain support (Fig. 6) was unsuitable for an SG installation and was therefore replaced by a screw mounting (Fig. 7), with one of the screws on each side being a measuring screw fitted with SGs.

The tensile force of the chains cannot be directly calculated from the strain measured in the shank of the screw, but instead comes from the change in the pre-stress force conspiring between the bracing of the plates and the screw.

The stress chart of the screwed connection (Fig. 8) shows that there are changes in the working force  $F_a$  superposed on the installation pre-stress force  $F_0$  and in the deformation state in the screw itself, as well as in the clamped components. This means that the working force can then only be determined by measuring the change in the pre-stress force of the screws if the stiffness constants both of screw  $c_1$  and of the clamped components  $c_2$

are known. In this situation, it is not possible to estimate  $c_2$  with sufficient accuracy.

This is why the entire measuring device is calibrated with the chains rotating freely on the basis of the known centrifugal force at the chain mounting. To make the calculation easier, the chain is modeled as a rotating straight body with constant mass distribution in the longitudinal direction, whereby:

$$F = m \cdot \varnothing \cdot r \quad (1)$$

With a chain mass of  $m = 8.2 \text{ kg}$ , a radius of  $r = 0.61 \text{ m}$  (distance of the center of gravity from the axis of rotation) and a speed of  $n = 750 \text{ rpm}$ , this results in:

$$F = 8.2 \text{ kg} \cdot 6168.5 \text{ s}^{-2} \cdot 0.61 \text{ m} = 30.8 \text{ kN}$$

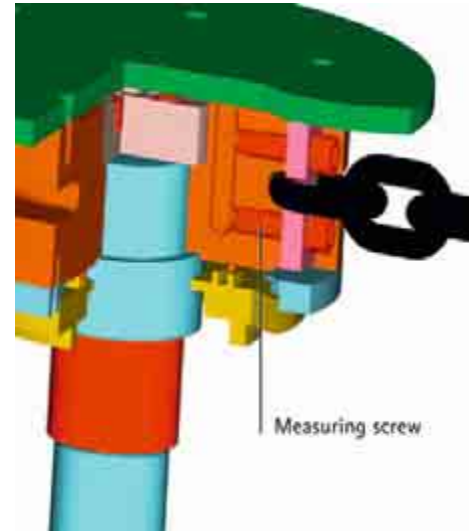
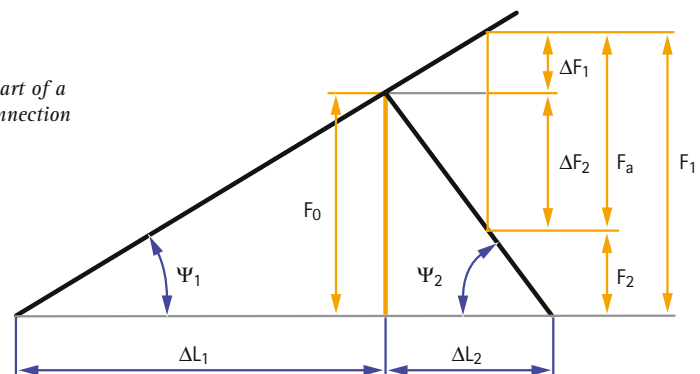


Fig. 7: Chain support with measuring screw

Fig. 8: Stress chart of a screw connection



$F_0$	Installation pre-stress force of the connection
$\Delta L_1$	Deformation (extension) of the screw caused by the installation pre-stress force
$\Delta L_2$	Deformation (compression) of the clamped components caused by the installation pre-stress force
$c_1 = \tan \Psi_1$	Screw stiffness constant
$c_2 = \tan \Psi_2$	Stiffness constant of the clamped components
$F_a$	Maximum axial working force of the connection
$\Delta F_1$	Part of the axial component of the working force additionally loading the screw
$\Delta F_2$	Part of the axial component of the working force relieving the clamped components
$F_1$	Maximum internal axial force in the screw
$F_2$	Residual pre-stress force of the clamped connection components

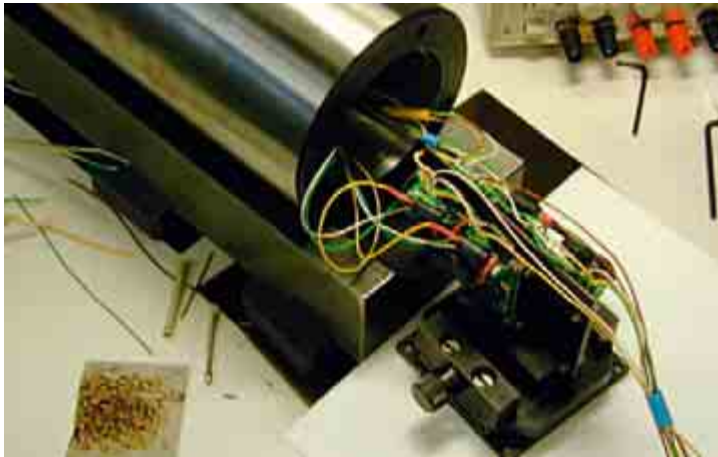


Fig. 9: Preamplifier installation in the hollow shaft end



Fig. 10: Slip ring transformer installation

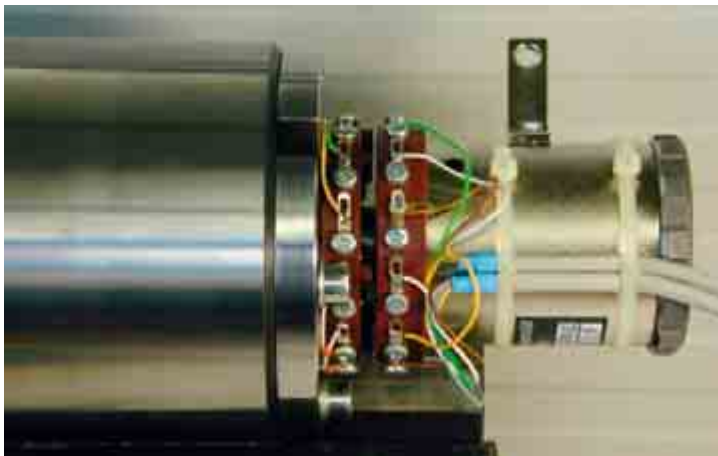


Fig. 11: Shaft end with fully wired slip-ring transformer

This centrifugal force loads both of the fastening screws, of which only one is executed as a measuring screw. The calibration process dictates that force is distributed evenly to both the screws, so that the strain value recorded by SGs at only one of the measuring screws under load from the centrifugal force corresponds to this force.

When measured values were recorded during test operation, it was discovered that temperature increases at the chain restraint were causing a change in the clamping conditions in accordance with Figure 8, which lead to a considerable increase in pre-stressing, so that the tensile forces of the chains could only be evaluated in starting mode.

Overall, this produced the general measurement channel configuration shown in Table 1.

Various commercially available transmission systems were tested for their suitability for transferring the measurement signals from the rotating shaft. The decision was made to use HBM's SK12 slip ring transformer as this is designed for the direct transmission of SG measurement signals. It is characterized by its low contact resistance of < 40 mΩ with a noise component of 2 mΩ.

To further improve the quality of the measurement signals, signal amplifiers were connected on the line side of the slip ring transformer. The amplifier modules are designed for connecting SG full bridges and return an output signal of ± 5 V at an input signal of ± 2 mV/V.

Measured quantity	Channels	Bridge type	SG type
Bending moment of the input shaft (on two axes)	2	Half bridge	6/120LY11
Torsional moment of the input shaft	1	Full bridge	3/120XY21
Tensile force of the chains (two sides)	2	Quarter bridge	KFG -1.5-120-C20-11

Tab. 1: General measurement channel configuration

They are installed in the end of the shaft in a hole made for this purpose. Completion resistors for half and quarter bridges could also be located here. Figures 9 to 11 show the installation of the amplifiers and the slip ring transformer.

The amplified signals were connected to an HBM MGCplus amplifier system with an AP 801 connection board for  $\pm 10\text{V}$  inputs and an ML801B amplifier module, with 8 channels available. HBM's catman® 4.0 software was used to control the amplifier, as well as to obtain, process and graphically display the measured values on a PC. The two systems (PC and measuring amplifier) communicate via a parallel interface in so-called EPP mode.

### Measurement results

The recycling machine was put into operation with the measurement technology installed and the tensile force sensors for the chain calibrated as described above. The torsional moment curve, shown in general terms in Figure 12, made the most important contribution to the analysis of pulverization.

Figures 13 and 14 show the torsional moment curve when disintegrating aluminum and steel, with the accompanying individual images from the high-speed film. The sequence of events during the disintegration process is clearly visible. By combining this with visual analysis, it was possible to define the end of material disintegration by lowering the torsional load by 20%.

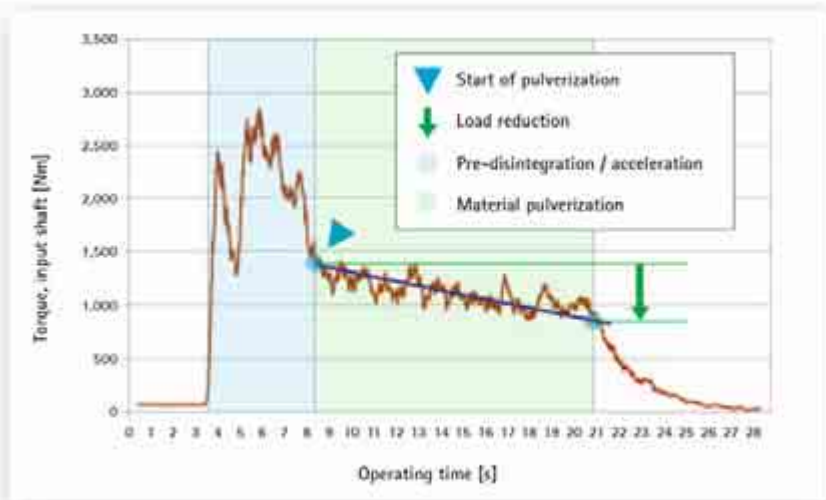


Fig. 12: General torsional moment curve during material pulverization

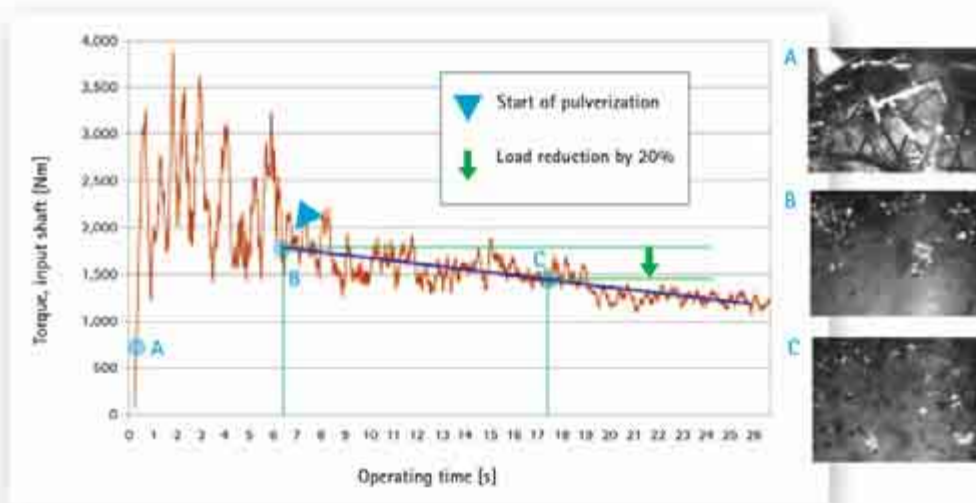


Fig. 13: Torsional moment during aluminum disintegration

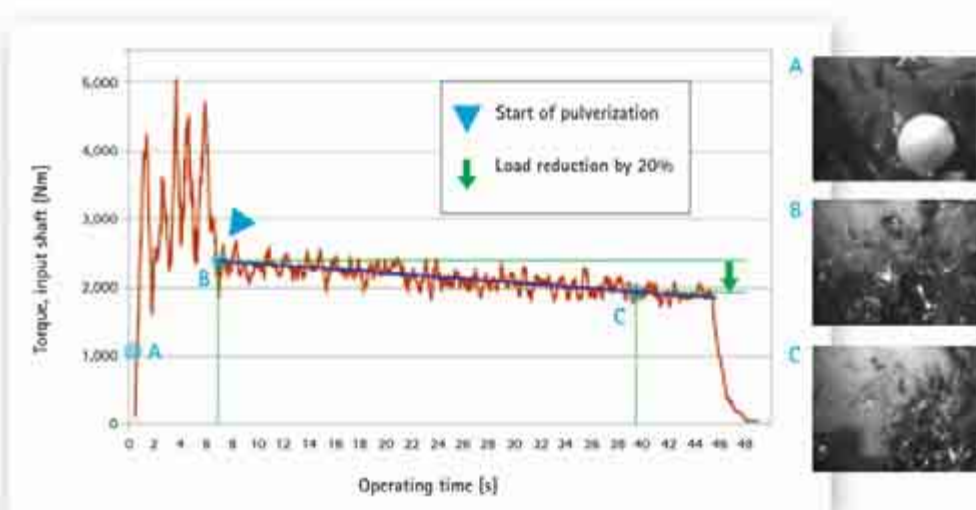


Fig. 14: Torsional moment during steel disintegration

It was also possible to obtain important information about the loads when putting in the material, that is to say, during fitting. The bending load curve (Fig. 15) returns a similar result after vectorial addition of the two measurement channels.

No reduction in load during material pulverization was detectable here, which indicates that the impact chains only supply energy rarely and evenly. The findings from the measurements were nevertheless valuable for working out standards for dimensioning the machine.

The tensile force curves in both chains shown in Figure 16 include the pre-stress forces of the screws. The rapid heating of the impact chains during the disintegration process heats up the screwed connection as well. The connection components then expand differently, which causes measurement errors. The measured values are therefore only displayed for the initial material pulverization range and must be analyzed critically.

### Practical experience and prospects

The test findings helped to improve understanding of the process of material pulverization and to develop a model of the predicted process. This particularly affects the measurement of torsional and bending moment at the input shaft under different operating conditions. The extremely difficult conditions made it difficult to measure the tensile forces of the chains. The vast increase in temperature during operation lead to measurement errors that were impossible to calculate. The thermal stress of the steel chain links during material pulverization is certainly so great that they glow red and some even melted at the ends. On the other hand, the technology used to transmit and record the measured values met all its expectations in full.

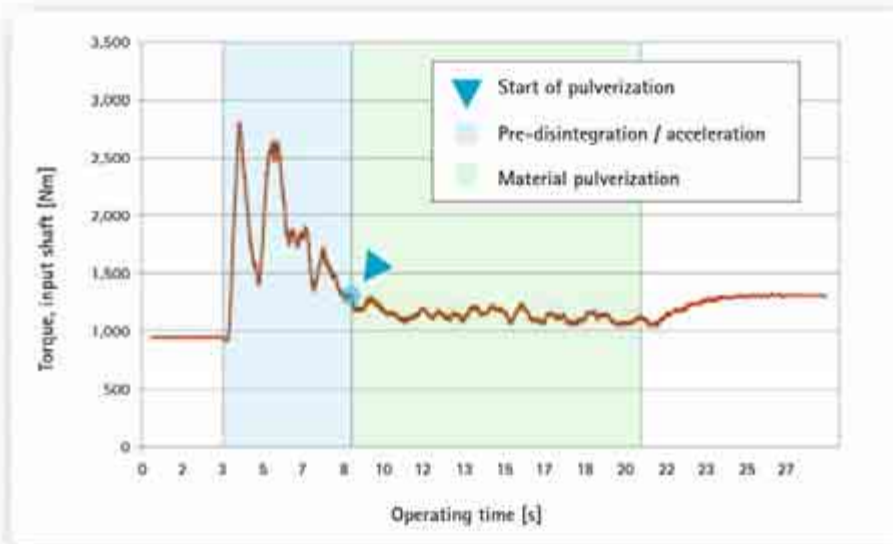


Fig. 15: General curve of the resultant bending moment during material pulverization

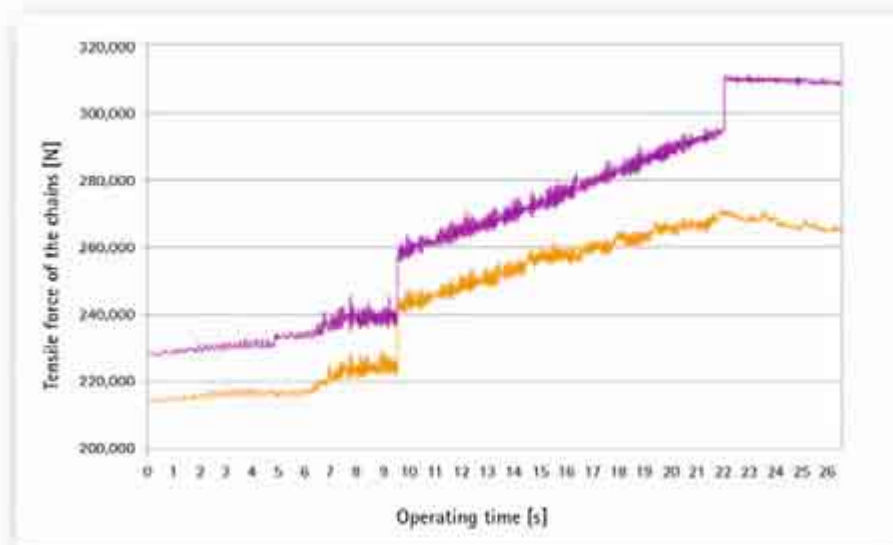


Fig. 16: Curve of the tensile forces of the chains during disintegration of car tires

# ram reports in applied measurement

## Stress analysis of human teeth crowns in terms of proper occlusions

Grzegorz Milewski, Cracow University of Technology, Poland

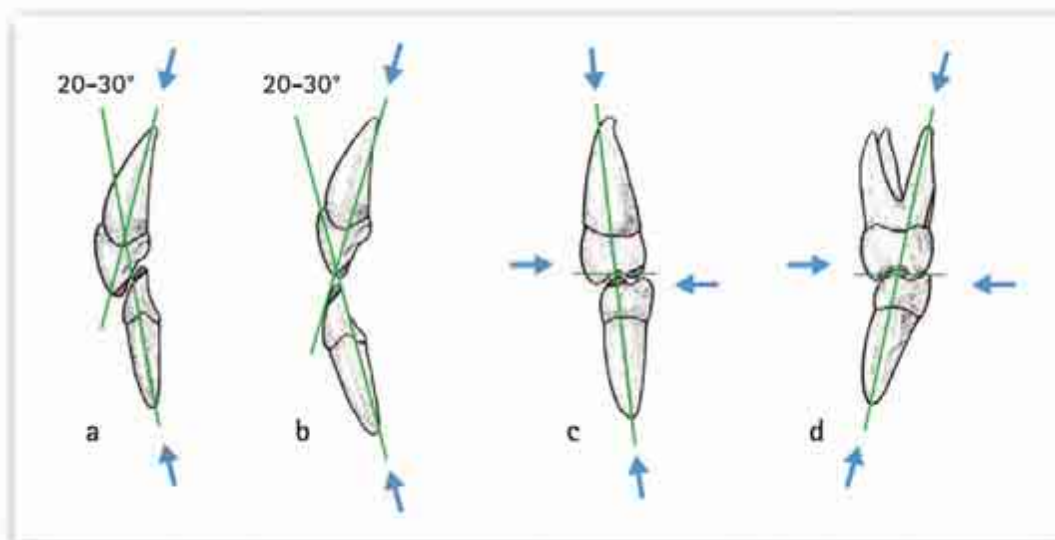


Fig. 1:  
Loadings for  
the anterior (a, b)  
and lateral teeth (c, d)

### Introduction

Standards of occlusion for human teeth are individually distinguishable and are determined by face shape, tooth location, the shape of the alveolar arch and the particular individual movements of the mandible during the physiological activities of biting and mastication (W. Lasinski [1], B. Kahl-Nieke [2]). However, only some types of occlusion, including the so-called edge-to-edge and end-to-end bites are considered to be proper. The features of the occlusal loadings corresponding to the above bite types are illustrated in Figure 1.

The investigation comprises loading experiments, including measuring strain with strain gages to analyze the deformation and load distribution in all groups of human teeth

crowns. Proper occlusal loadings were assumed for the simulated masticatory movements of lateral teeth. The results of the experiments are compared with the findings from numerical investigations using the finite element method (FEM). The results obtained by experimentation were consistent with the numerical findings. The investigations provide information about the stress on different areas of the hard tooth material (enamel) during masticatory and occlusal loading.

### Material and methods

Stress tests were performed for all the teeth groups (incisors, canines, premolars and molars). In total there were 60 original teeth available, that had been removed because of peridontitis or orthodontic indications. All the

teeth samples were prepared in the Institute of Dentistry of Collegium Medicum of the Jagiellonian University. The strength tests on the original teeth corresponding to the above types of occlusion were done on an INSTRON 8511.20 type materials tester in the Division of Experimental Mechanics and Biomechanics of the Cracow University of Technology. The experiments took place at room temperature and standard humidity. All the teeth samples were kept in Ringer solution until they were needed for testing.

At the same time, investigations were carried out for the relevant teeth groups on teeth models prepared with strain gages. The test setup for these model experiments comprised an INSTRON 4456 materials tester, a UPM 40 A multipoint measuring device and a DMC measuring amplifier (both HBM), as shown in

Figure 2. The SG rosettes used in the experiments were cemented to the teeth models with X60 fast-setting adhesive.

All the characteristic surfaces of the teeth were taken into account in the choice of measuring points (that is to say, mesial, distal, buccal and lingual).

The experiments were performed with sequential loading and unloading components in the range 5 N to 200 N, depending on the type of tooth. The teeth models were made of epoxy resin and were increased in size on a scale of 5:1. The deformation and stress values were converted to the original teeth in accordance with the laws of similarity mechanics, taking the scale into account, and with the ratio of the moduli of elasticity:

$$\frac{E_{\text{Enamel}}}{E_{\text{Epoxy resin}}} = 30$$

The Poisson constants are the same here:

$$\nu_{\text{Enamel}} = \nu_{\text{Epoxy resin}}$$



Fig. 2: Test setup and teeth models with SGs for investigating the anterior (a, b) and lateral (c, d) teeth groups in accordance with the load schemes in Fig. 1



Teeth group	Type of occlusion	Ultimate force $F_u$ [N]	Scatter [N]
Upper mesial incisor	proper occlusion	620	350 - 810
	edge-to-edge bite	670	420 - 900
Upper distal incisor	proper occlusion	340	290 - 440
	edge-to-edge bite	390	190 - 680
Lower incisor	proper occlusion	280	180 - 500
	end-to-end bite	470	350 - 620
Upper and lower canine	proper occlusion	690	380 - 950
	end-to-end bite	1,290	730 - 1,540
Lower premolar	proper occlusion	1,820	1,370 - 2,120
	mastication	240	220 - 250
Upper premolar	proper occlusion	770	580 - 950
	mastication	260	180 - 320
Lower molar	proper occlusion	2,140	1,150 - 3,120
	mastication	510	290 - 700
Upper molar	proper occlusion	168	970 - 2,060
	mastication	520	330 - 810

Tab. 1: Measured values for the critical loading (ultimate force) of the individual teeth groups in the maxilla and mandible, for typical, proper occlusions

After determining the deformation and stress fields by experiment using strain gages, numerical analyses were performed with the ANSYS® FEM software package.

This combination of the two methods made it possible to:

- ensure the accuracy of the results by comparing the two methods (experimental and numerical)
- determine which points on the teeth crowns were subjected to the most stress and as a result, create guidelines for carrying out fillings in conservative dentistry

### Results

In strength tests on original teeth, the following parameters were defined:

- $F_c$  : Force, at which the first microcracks or crumbles appear
- $F_u$  : Ultimate force
- $W_f$ : Work to fracture

Table 1 shows the average values of the ultimate force and their scatter. The ultimate force is the force that ultimately destroys the individual teeth crowns.

Please note that the relatively large scatter of results was due to the fact that, just as in nature, the individual teeth are not identical. So there were anatomical differences of size and shape in the individual teeth groups, as well as some of the teeth already having initial enamel fractures and the beginnings of caries. Nevertheless, the results obtained are reliable.

The measured maximum values of the occlusal forces that differ at different points on the human dental arches, are in accordance with the reference data (J. W. Osborn, F. A. Baragar [3], T. W. P. Koriath, et al. [4]).

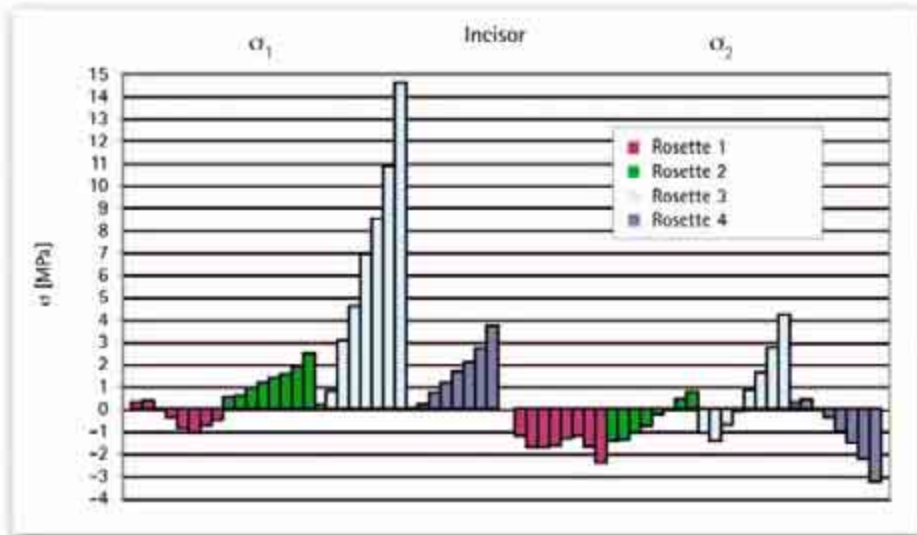


Fig. 3: Primary stresses  $\hat{\sigma}_1$  and  $\hat{\sigma}_2$  [MPa] in the incisor crown in different load steps

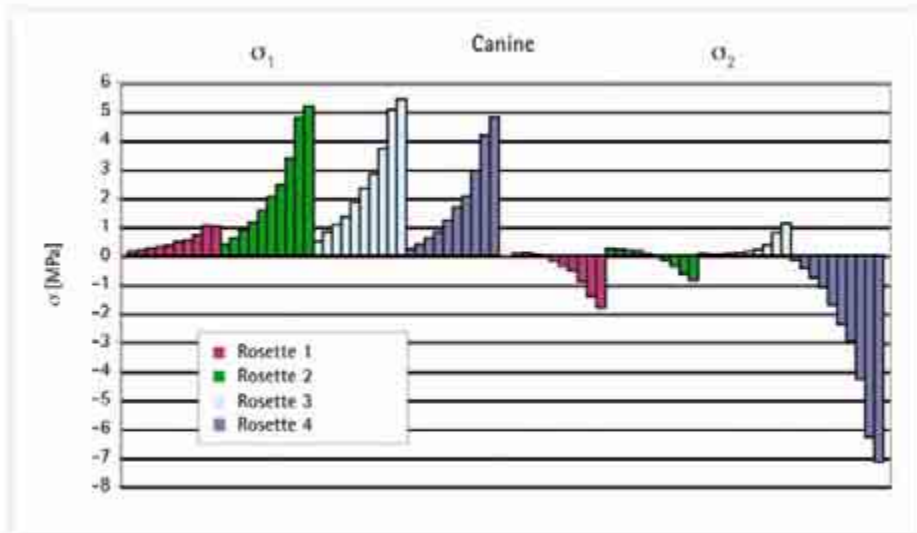


Fig. 4: Primary stresses  $\hat{\sigma}_1$  and  $\hat{\sigma}_2$  [MPa] in the canine crown in different load steps

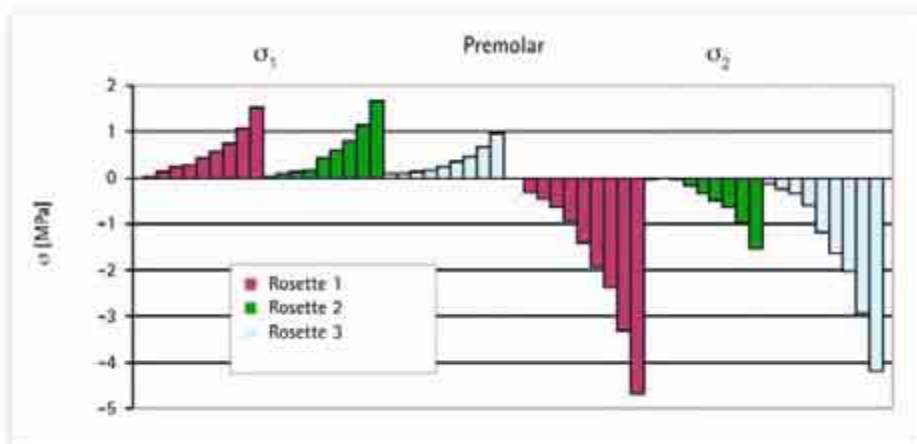


Fig. 5: Primary stresses  $\hat{\sigma}_1$  and  $\hat{\sigma}_2$  [MPa] in the premolar crown in different load steps

The model experiments with strain gages involved sequential loading and unloading. The forces for incisors were in the range 10 to 200 N, for canines 10 to 110 N, for premolars 10 to 100 N and for molars 5 to 70 N. At these loads, there was elastic deformation for all types of teeth and practically linear hysteresis loops. Figures 3 to 6 show the development of primary stresses  $\hat{\sigma}_1$  and  $\hat{\sigma}_2$  in the different areas of the individual teeth, already converted to the original teeth.

These results show that the areas of maximum stress lie between the base of the crown and the gingival line. This applies to incisors, canines and premolars. Only in the case of molars are there higher stress values occurring in the areas close to the cusps. The highest stress values in the crown base of incisors occur on the lingual and buccal surfaces. On the lingual surface, the highest stress values at a tooth loading of 200 N are 15 MPa. In the case of canines, it is the lingual surface at the crown base that is under the most stress. At a loading of 110 N, the maximum stresses here exceed 7 MPa, with 5 MPa at the buccal side. The mesial and distal surfaces also seem to be highly stressed, at more than 5 MPa. In the case of the incisors, the stress on these surfaces is only a third to a half as much as that on the lingual side. Typical for molars and premolars is a relatively even stress of all the characteristic surfaces. The primary stresses at the crown base here are about 4 MPa, at a loading of 70 N for molars and 100 N for premolars.

In the case of molars, the highest stress levels are in the crown cusp areas. The primary stresses here are in excess of 16 MPa. In the case of premolars, the cusps are under less load. The primary stresses here are about 2 MPa.

Comparing the stresses of the individual teeth groups with one another therefore looks very interesting. Figure 7 shows the maximum values of primary stresses  $\hat{\sigma}_1$  and  $\hat{\sigma}_2$ . The individual teeth are each simultaneously loaded at 70 N. This gives the following sequence when putting the teeth in order of stress level: molars, canines, incisors and premolars. This result matches the clinical observations very well.

The experimental and numerical results were compared for the canines. The geometry of these teeth was measured exactly by means of a three-dimensional scanning procedure (Leitz PMM 12106 coordinate measuring device) and transferred to an FE network by the Mechanical Desktop® and FEMAP® software packages (Fig. 8).

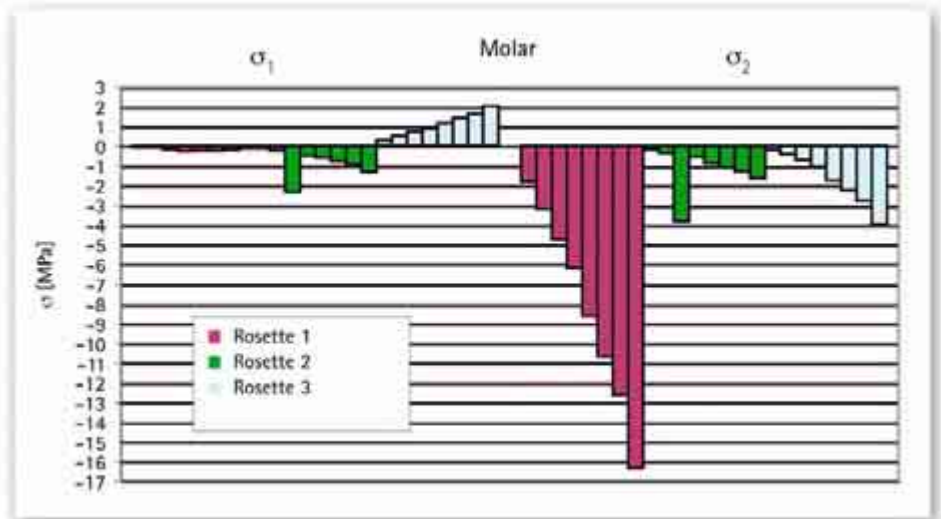


Fig. 6: Primary stresses  $\hat{\sigma}_1$  and  $\hat{\sigma}_2$  [MPa] in the molar crown in different load steps

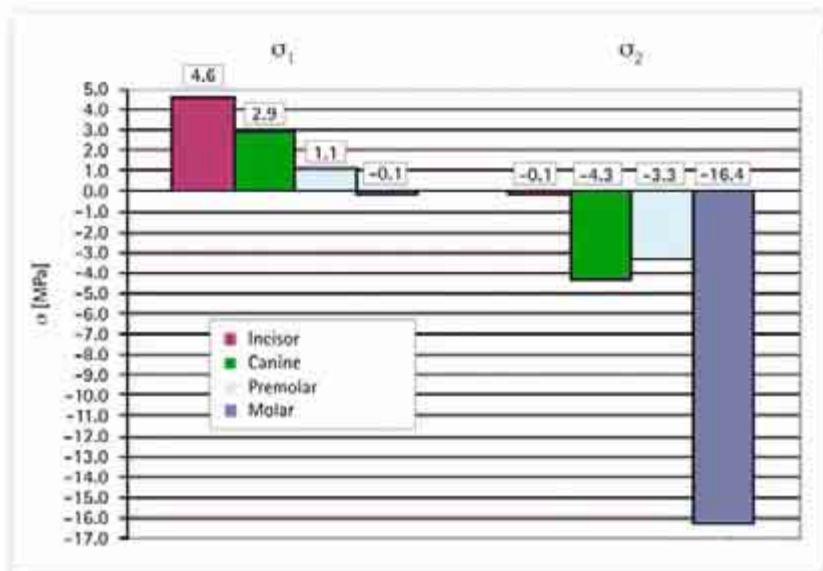


Fig. 7: Comparison of the maximum values of the primary stresses  $\hat{\sigma}_1$  and  $\hat{\sigma}_2$  in tooth enamel at an occlusal force of 70 N, broken down by teeth groups

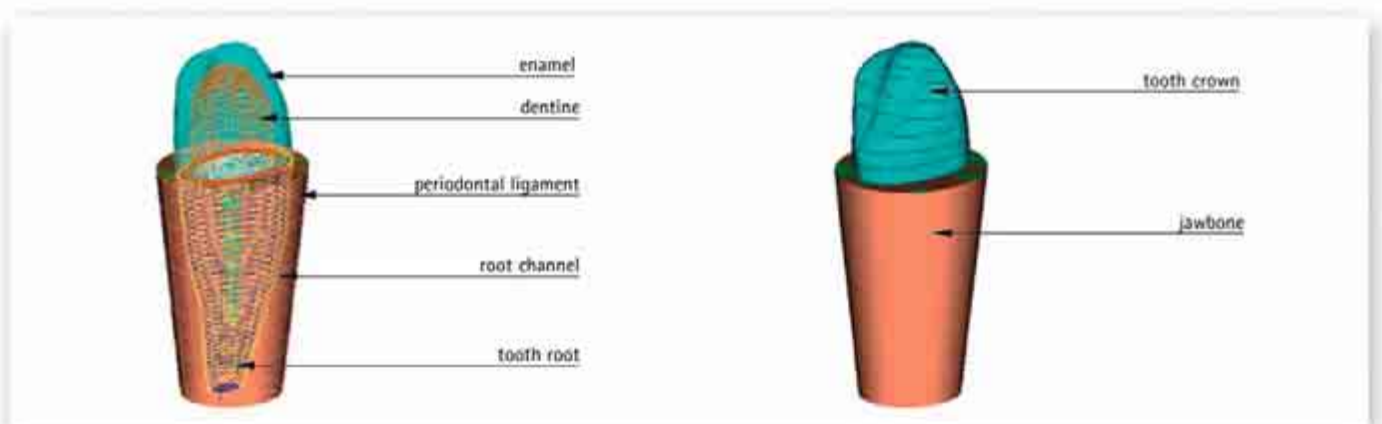


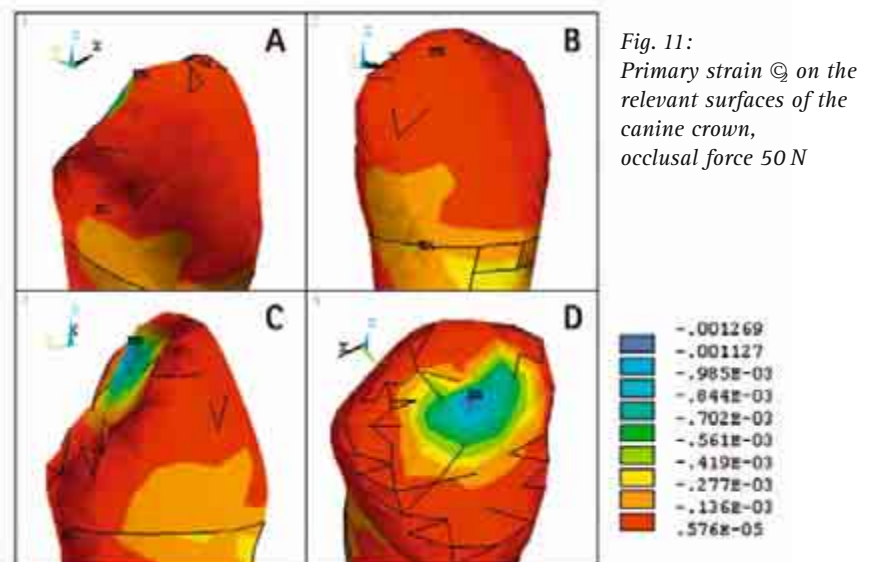
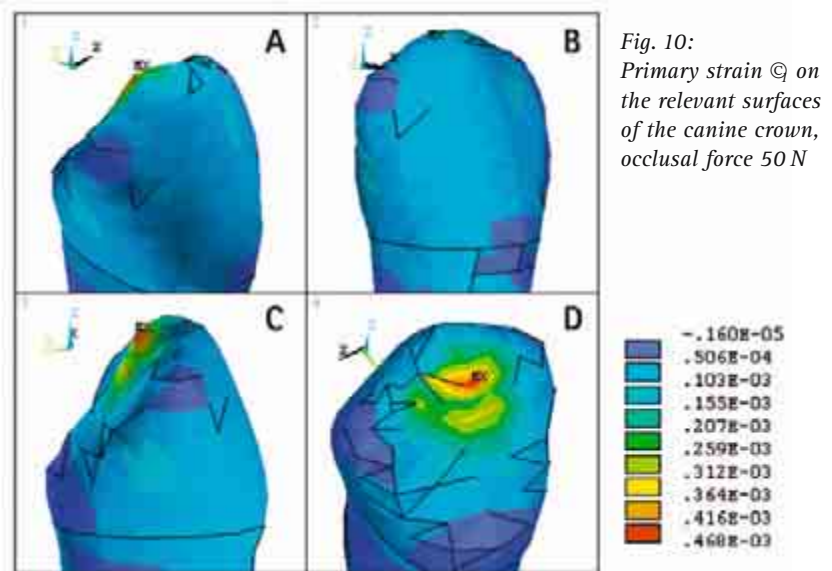
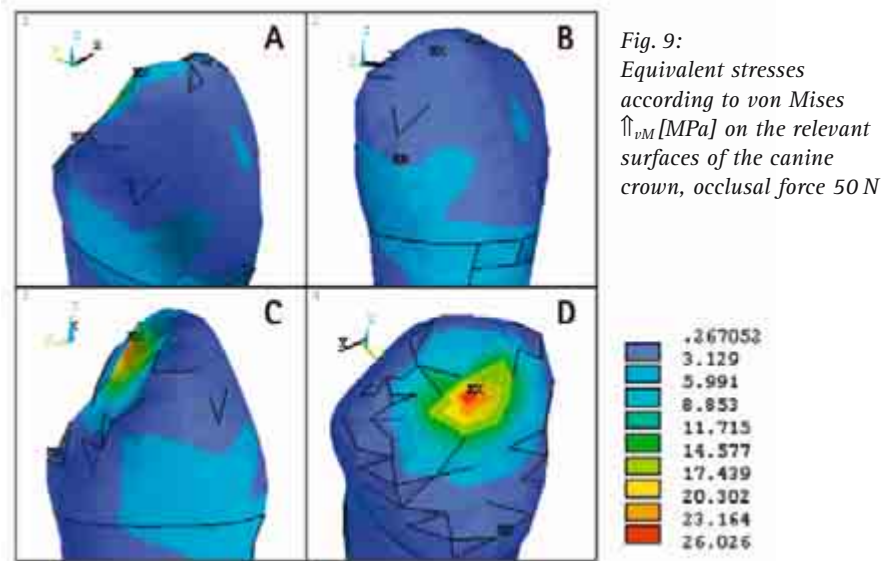
Fig. 8: FE model of the canine geometry, generated with the Mechanical Desktop® and FEMAP® software on the basis of a 3-D scan of a real tooth

Figures 9, 10 and 11 show the equivalent stresses according to von Mises  $\hat{\sigma}_{vM}$ , and the primary strains  $\epsilon_x$  and  $\epsilon_y$  on the four relevant surfaces of the canine crown. Table 2 contains a comparison of the experimental and numerical results for a canine at an occlusal force of 50 N. The SG rosettes are attached to the crown of the tooth as follows (crown area of the tooth):

- 1: buccal surface at top crown edge
- 2: distal surface at base of crown
- 3: buccal surface at base of crown
- 4: lingual surface at base of crown of the canine.

The material constants used in the numerical calculations for dentine and enamel are taken from R. G. Craig, F. A. Peyton [5] and R. G. Craig [6].

The results are very consistent with one another. For stresses, the average error is 12%, for deformations, 22%. An analysis of the results indicates that the areas of the teeth crowns under the greatest stress are the base of the crown near the gingival line. This also applies to incisors, canines and premolars. Only in the case of molars are there higher stress values occurring in the areas close to the cusps. It should be pointed out that it was not possible to directly investigate the mastication area in the experiments, as it is not possible to attach the SG rosettes directly onto the occlusal teeth contact areas.



Crown area of the tooth	$\epsilon_x$ [ $\times 10^{-6}$ ]		$\epsilon_y$ [ $\times 10^{-6}$ ]		$\sigma_{VM}$ [MPa]	
	SG	FEM	SG	FEM	SG	FEM
1	44	68	-43	-47	0.92	1.24
2	150	96	-57	-113	2.53	2.92
3	215	124	-95	-116	2.72	2.81
4	181	131	-217	-179	4.36	4.71

Tab. 2: Primary strains  $\epsilon_x$ ,  $\epsilon_y$  and equivalent stress  $\sigma_{VM}$ , canines with occlusal force  $F = 50\text{ N}$ , comparison between experiment (SG measurement) and theory (FEM)

Tooth structure	Composite material for reconstruction of the tooth crown	$\sigma_{max}$ [MPa]	Comment	
Dentine	chemical and light-cured composites	11-35	with bonding system	
	glass-ionomeric cements	traditional	4-6	without bonding system
		hybrid	10-12	without bonding system
Enamel	chemical and light-cured composites	10-22	with bonding system	
	glass-ionomeric cements	5-12	without bonding system	

Tab. 3: Shear strength values for modern composite dental materials

The quality of the adhesive bond between the filling and the tooth material has a crucial role to play in assessing the durability of teeth fillings. The shear stresses that occur are commonly regarded as a criterion for the durability of a tooth filling [Z. Janczuk [7], E. Jodkowska [8] and [9], C. M. Sturdevant et al. [10]].

Table 3 gives the shear strength values for a selection of modern composite dental materials.

The basic compatibility of the experimental and numerical results allows us to conclude that even complicated shapes and stresses can be calculated numerically. This applies in par-

ticular to the attachment areas of dental fillings and other reconstructions (Fig. 12).

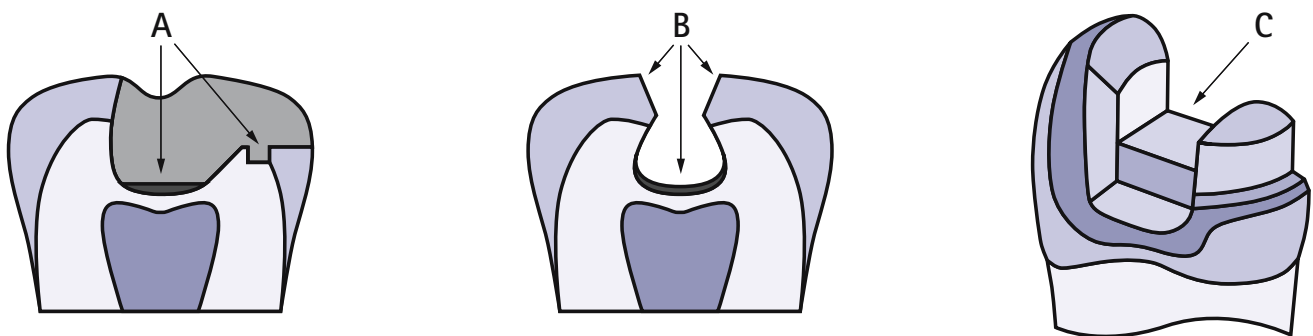


Fig. 12: Typical attachment surfaces and elements for the reconstruction of tooth crowns in conservative dentistry (a, b, c)

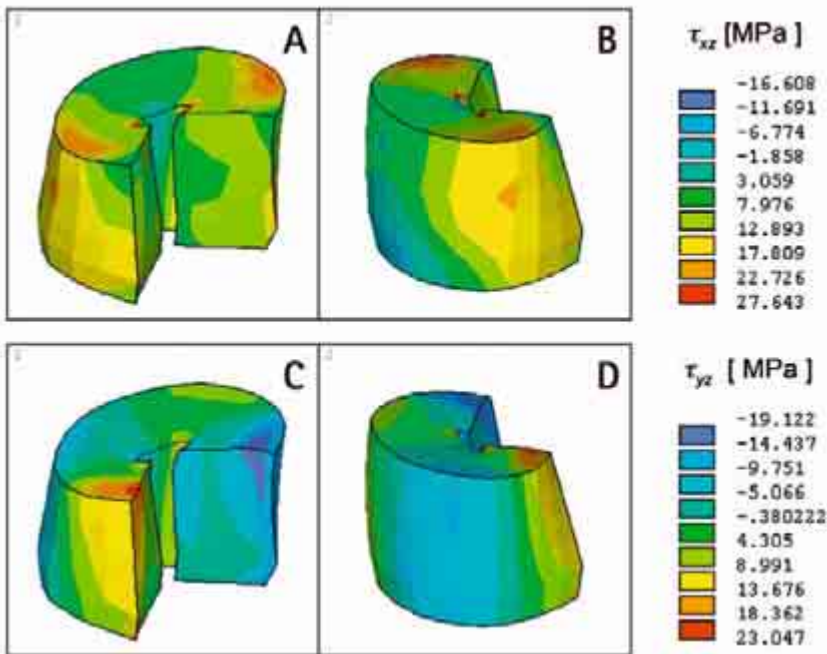


Fig. 13: Distribution of shear stresses  $\tau_{xz}$  and  $\tau_{yz}$  in the enamel of a tooth crown, occlusal force 500 N

Figure 13 presents as an example the distribution of the shear stresses  $\tau_{xz}$  and  $\tau_{yz}$  in the enamel of an incisor crown at an occlusal force of 500 N with a proper occlusion (cross-section and longitudinal section through the crown of the tooth). The maximum values of the calculated shear stresses exceed the shear strength values of composite materials given in Table 3, which is to be taken into account when preparing the cavities for filling. Further details can be found in the paper by G. Milewski [11].

## Conclusions

By a combination of experimental investigations on tooth models using SG rosettes and numerical FE simulations, it is possible to reliably estimate and evaluate the stresses in teeth at different occlusal loadings. Thanks to the basic compatibility of the results of these two methods, it was also possible to use the numerical models to calculate the strength of fillings in modern conservative dentistry. This enables the stress distribution in the tooth material to be calculated, which is an important criterion for the selection of cavity reconstruction methods for tooth crowns.

## References

- [1] W. Lasinski: Anatomia głowy dla stomatologów, PZWL, Warszawa 1978.
- [2] B. Kahl-Nieke: Wprowadzenie do ortodoncji, Urban & Partner, Wrocław 1999.
- [3] J. W. Osborne, F. A. Baragar: Predicted activity of human muscles during clenching derived from a computer assisted model, *Journal of Biomechanics*, vol. 18, no. 5 (1985), pp. 599 – 612.
- [4] T. W. P. Koriath, T. W. Waldron, A. Versluis, J. K. Schulte: Forces and moments generated at the dental incisors during forceful biting in humans, *Journal of Biomechanics*, vol. 30, no. 6 (1997), pp. 631 – 633.
- [5] R. G. Craig, F. A. Peyton: Elastic and mechanical properties of human dentin, *Journal of Dental Research*, vol. 37, no. 4 (1958), pp. 710 – 718.
- [6] R. G. Craig: *Restorative Dental Materials* (9th ed.), C.V. Mosby, Saint Louis 1993.
- [7] Z. Janczuk: *Stomatologia zachowawcza – zarys kliniczny*, PZWL, Warszawa 1995.
- [8] E. Jodkowska, L. Wagner: Ocena porównawcza wiązań na scinanie zębiny z kompozytami, *Stomatologia Współczesna*, no. 5 (1998), s. 341 – 343.
- [9] E. Jodkowska: Wytrzymałość na scinanie wiązań pomiędzy twardymi tkankami zęba a wybranymi materiałami, III Sympozjum Inżynieria Ortopedyczna i Protetyczna, Białystok 2001, s. 95 – 99.
- [10] C. M. Sturdevant, T. M. Roberson, H. O. Heyman, J. R. Sturdevant: *The Art and Science of Operative Dentistry*, C.V. Mosby, Saint Louis 1995.
- [11] G. Milewski: Wytrzymałościowe aspekty interakcji biomechanicznej tkanka twarda-implant w stomatologii, *Wyd. Politechniki Krakowskiej*, s. *Mechanika* nr 89, Kraków, 2002.

# ram reports in applied measurement

## Mechanical and thermal strain

Martin Stockmann

The change in the length of a solid relative to its original length is, in a finite presentation, designated as technical strain  $\epsilon$  in accordance with equation 1 and in a differential presentation, designated as natural strain  $\varphi$ , in accordance with equation 2 (see [1]).

$$\epsilon = \frac{l_1 - l_0}{l_0} = \frac{\Delta l}{l_0} \quad (1)$$

$$\varphi = \int_{l_0}^{l_1} \frac{dl}{l} \quad (2)$$

If you observe the physical cause of this purely geometrically defined quantity, it is possible to establish that exposure both to the effects of external force and to changes in temperature result in strain. This is designated mechanical or thermal strain, depending on its cause. These two components often occur together and displacement and strain sensors that work purely geometrically cannot evaluate or mea-

sure them separately. On the other hand, in experimental stress analysis, when defining the reaction of components to external mechanical forces or in weighing technology, when the mass of a body is derived from its force due to weight at a known gravitational constant, it is important to define only the mechanical strain.

### Thermal strain

When the temperature rises in an independent solid, it expands evenly in all directions (Fig. 1). On condition that there is equal access in all directions, the extent of this thermal expansion is described by:

$$\epsilon_x^{th} = \epsilon_y^{th} = \epsilon_z^{th} = \alpha^{th} \cdot \Delta T \quad (3)$$

and in many cases, this condition is easily met.

The linear expansion coefficient  $\alpha^{th}$ , which is assumed to be constant here, is dependent on the material involved and is within the range  $10^{-6} \leq \alpha^{th} \leq 10^{-1}$ .

If you observe the overall expansion of crystalline materials (e.g. metals) from absolute zero  $T_0$  to melting point  $T_S$ , this produces a value which is virtually the same for many materials, of:

$$\epsilon_{gesamt}^{th} |_{T_0 \Rightarrow T_S} = 0.02 \quad (4)$$

So it is possible, in the form of equation 5, to specify a relationship between the expansion coefficients and the melting temperature of a metal in °C:

$$\alpha^{th} = \frac{0.02}{T_S + 273} \quad (5)$$

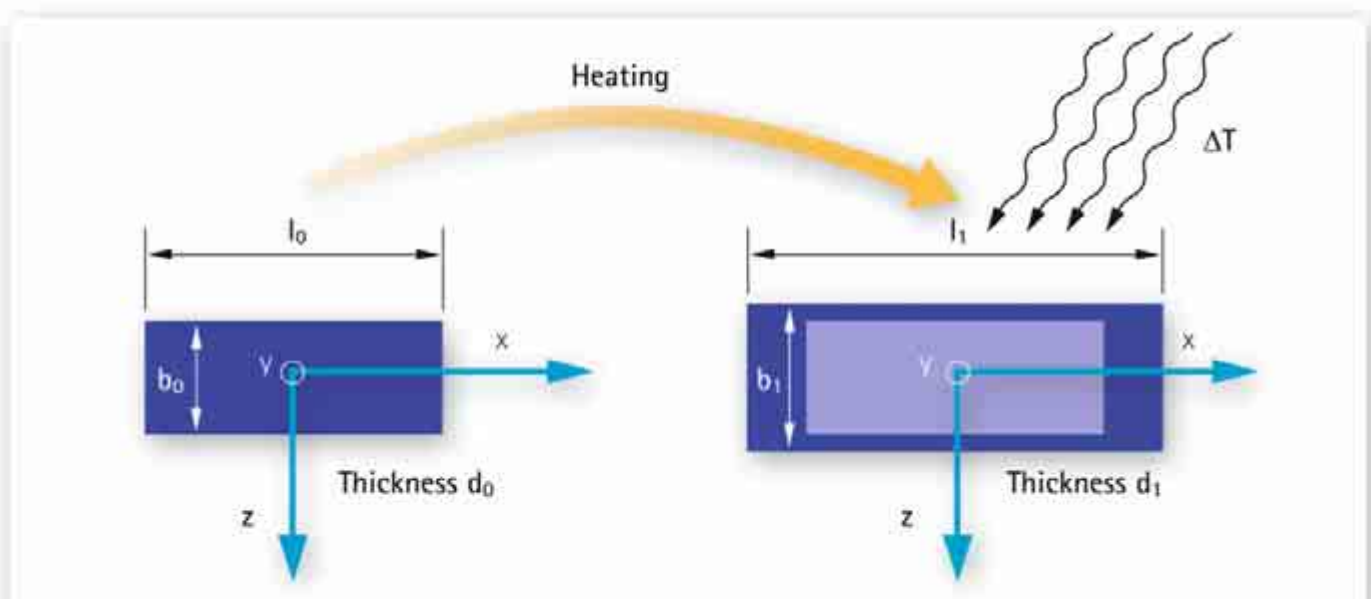


Fig. 1: Thermal strains as a result of heating

Figure 2 shows this correlation, initially described by Eduard Grüneisen, by means of the measured values of four metals to which equation 5 applies.

### Mechanical strain

If solids are put under stress by external forces, their shape changes. That is to say, there are changes in the length and angle of the original shape subject to the load and to the properties of the material. This is shown in Figure 3 for the simple load scheme of elastic deformation in a tension bar.

The mechanical strains for this situation are defined by:

$$\epsilon_x^{\text{mech}} = \frac{\sigma_x}{E} = \frac{F}{E \cdot A} \quad (6)$$

... and ...

$$\epsilon_y^{\text{mech}} = \epsilon_z^{\text{mech}} = -\nu \cdot \epsilon_x^{\text{mech}} \quad (7)$$

... where E is the modulus of elasticity and  $\nu$  is Poisson's ratio. This allows the external force F to be calculated from the mechanical strain.

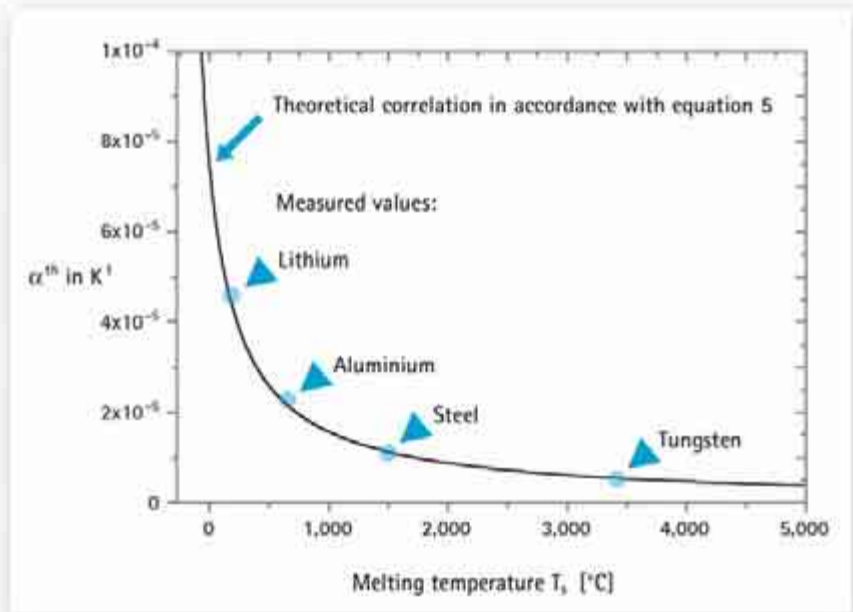


Fig. 2: Correlation between the thermal expansion coefficient /  $^{th}$  and the melting temperature  $T_s$

### Separate evaluation of the mechanical strain

As the thermal and the mechanical strain are cumulative, it is difficult to evaluate the mechanical strain separately. In SG measurement technology, two different methods of compensation are applied.

The first method of compensation utilizes a property of the WHEATSTONE bridge circuit that is used to measure the change in resistance of a strain gage (Fig. 4). The relative changes in resistance of the individual resistances arranged there appear in positive or negative pairs in bridge equation 8.

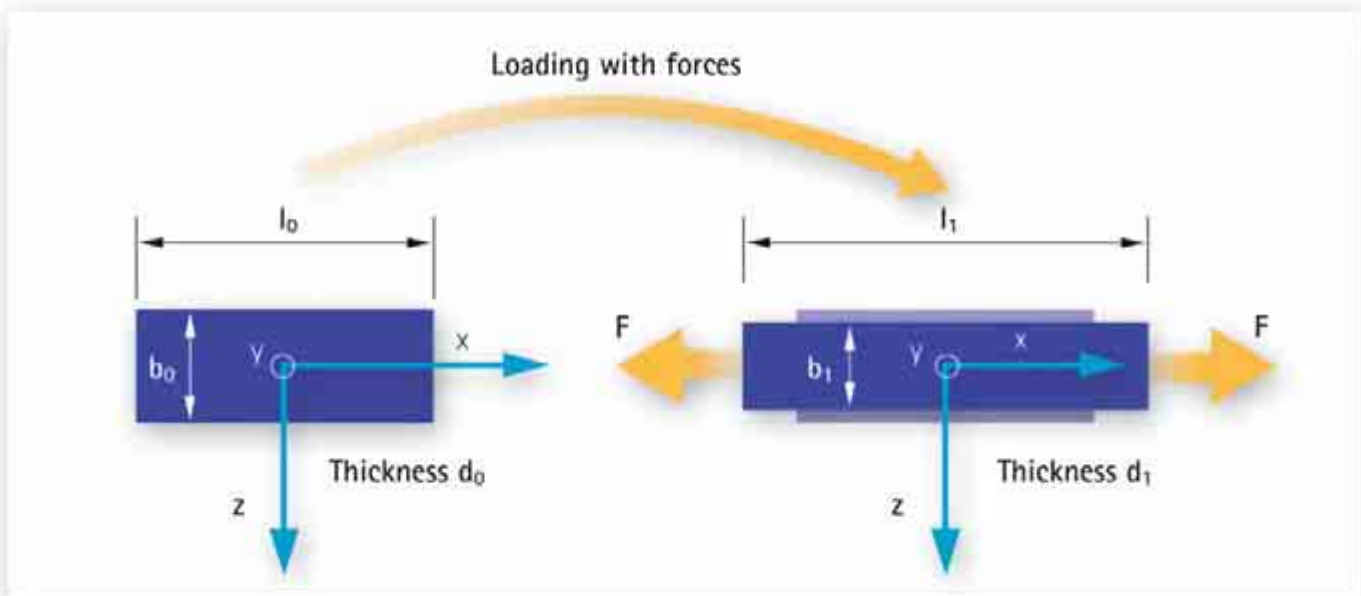
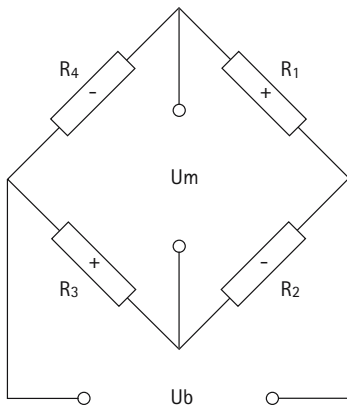


Fig. 3: Mechanical strains as a result of external forces



$$\frac{U_m}{U_b} = \frac{1}{4} \left( \frac{\Delta R_1}{R_0} - \frac{\Delta R_2}{R_0} + \frac{\Delta R_3}{R_0} - \frac{\Delta R_4}{R_0} \right) \quad (8)$$

Fig. 4: WHEATSTONE bridge circuit

Thermal strain in all the SGs, presupposing the same temperature, always causes changes in resistance with the same mathematical sign, so compensation options are numerous. One of these options is explained here, by way of example. For example, if resistance R<sub>1</sub> represents the actual active SG installed on a component, it is exposed simultaneously to mechanical and thermal strain. In addition, if resistance R<sub>2</sub> is also implemented as an SG, but is the "dummy" on a non-mechanically loaded blank panel that is at the same temperature as the component, and if resistances R<sub>3</sub> and R<sub>4</sub> are fixed resistances, then:

$$\frac{U_m}{U_b} = \frac{1}{4} \left( \frac{\Delta R_1^{mech}}{R_0} + \frac{\Delta R_1^{th}}{R_0} - \frac{\Delta R_2^{th}}{R_0} \right) \quad (9)$$

Presupposing that the thermal expansion coefficients of the component and the blank plate are also the same and that the SG has identical properties, then:

$$\frac{\Delta R_1^{th}}{R_0} = \frac{\Delta R_2^{th}}{R_0} \quad (10)$$

... and with ...

$$\frac{U_m}{U_b} = \frac{1}{4} \left( \frac{\Delta R_1^{mech}}{R_0} \right) \quad (11)$$

... the thermal strain is fully compensated.

A second compensation, not connected in any way with the WHEATSTONE bridge circuit, arises from adapting the mechanical and electrical properties of the conductor material to the thermal expansion coefficients of the component material.

Because the thermal expansion coefficients in the component and in the conductor are different (Fig. 5), when the temperature of the overall system changes, there is mechanical strain in the conductor:

$$\epsilon_L^{mech} = \epsilon_B^{th} - \epsilon_L^{th} = (\alpha_B^{th} - \alpha_L^{th}) \Delta T \quad (12)$$

Certainly the conductor itself has a temperature response even in a mechanically unloaded state, which can be expressed by ...

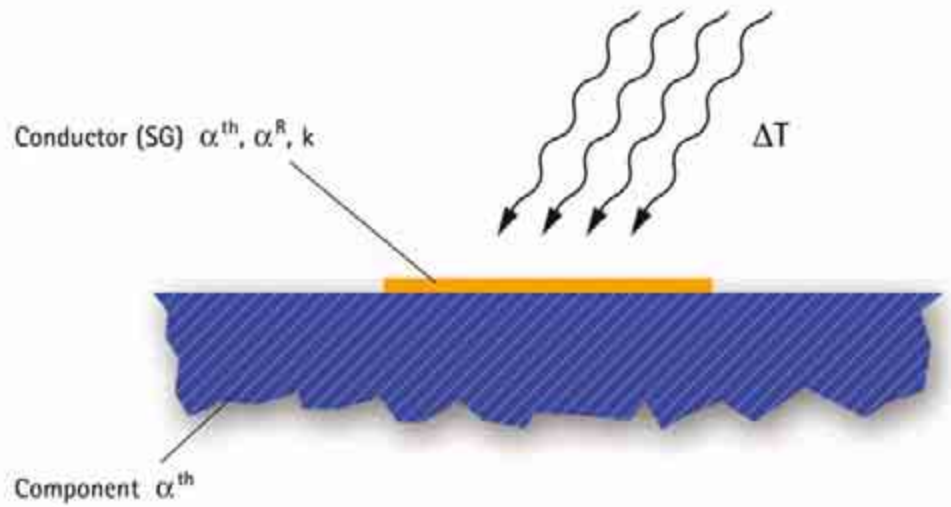


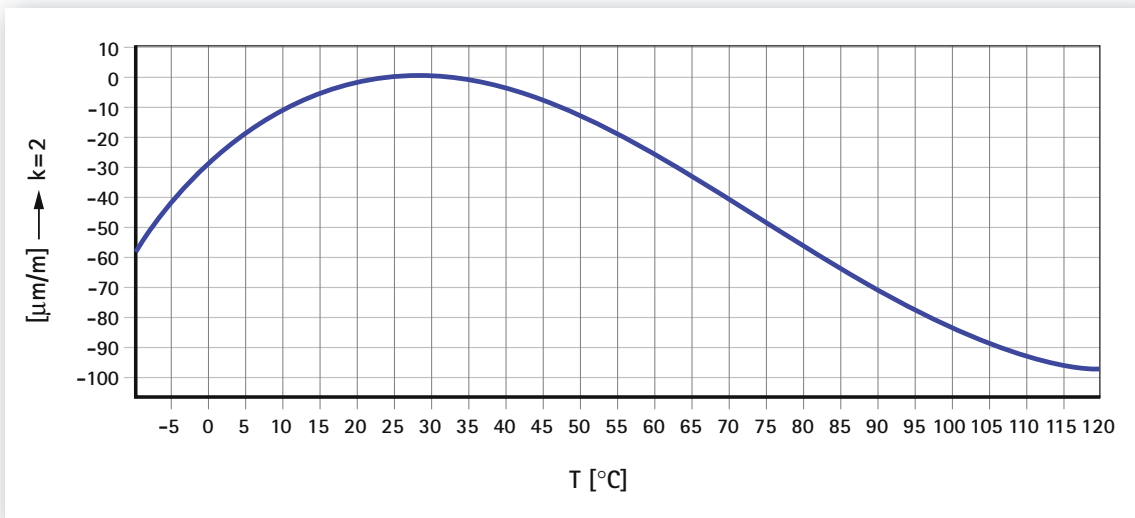
Fig. 5: Idealized representation of a conductor (SG) installed on a component, during a change in temperature

$$\frac{\Delta R}{R_0} = \alpha^R \Delta T \quad (13)$$

... where α<sup>R</sup> is the temperature coefficient of the resistance. It therefore follows with ...

$$\frac{\Delta R}{R_0} = [k (\alpha_B^{th} - \alpha_L^{th}) + \alpha^R] \Delta T \quad (14)$$

... that the resistance of a conductor prepared on a component changes when there is a change in temperature.



$$\epsilon_s(T) = -28.3 + 2.33 \cdot T - 5.19 \cdot 10^{-2} \cdot T^2 + 2.31 \cdot 10^{-4} \cdot T^3 \pm 0.3 (\mu\text{m/m}) \text{ } ^\circ\text{C}^{-1}$$

Fig. 6: Graphical and analytical representation of the temperature response of the LY41-6/120 strain gage, adapted to steel with  $\alpha_B^h = 10.8 \cdot 10^{-6} \text{K}^{-1}$

On the condition that this thermally induced fraction of the total change in resistance is to disappear, it is possible to specify a formal correlation between the thermal expansion coefficient of conductor and component and a requisite temperature coefficient of the resistance:

$$\frac{\Delta R}{R_0} = 0 \Rightarrow \alpha^R = k(\alpha_L^{th} - \alpha_B^{th}) \quad (15)$$

SG resistance materials such as constantan or Karma alloy have the property that  $\alpha^R$  can be set by a defined heat treatment of the cold-rolled foil. This makes it possible to comply with equation 15 for different component materials.

All three of the temperature coefficients ( $\alpha^R$ ,  $\alpha_L^{th}$ ,  $\alpha_B^{th}$ ) are only constants within a narrow range of temperatures, so that the temperature adaptation obtained for a component material only ever applies to this temperature range.

Strain gage manufacturers therefore specify this temperature adaptation as a curve and frequently as a polynomial as well. This information is displayed in Figure 6 for HBM's LY41-6/120 strain gage, adapted to steel with  $\alpha_B^h = 10.8 \cdot 10^{-6} \text{K}^{-1}$ .

This clearly shows that with an initial temperature of 20 °C and an increase in temperature of 20 K to 40 °C, the display is restricted to  $\epsilon_s \approx 3 \mu\text{m/m}$ .

On the other hand, the thermal strain of the component is  $\epsilon_B^h = 216 \mu\text{m/m}$ .

In an extended temperature range, it is possible to reduce the measurement error resulting from the remaining residual temperature response by using the specified polynomial.

The compensation methods described here reflect the advanced development status of strain gage technology and are a considerable help in minimizing measurement uncertainty in experimental stress analysis and in trans-

ducers. The two methods are frequently used in combination and can also be supplemented by additional compensation measures (see [2]), especially for demanding requirements, as is often the case with transducers.

## References

- [1] Martin Stockmann: Technische und natürliche Dehnung, MTB 2/2003, pages 18-19
- [2] HBM house journal: Der Weg zum Messgrößen-aufnehmer – ein Leitfaden zur Anwendung der HBM K-DMS und der Zubehörkomponenten

You are invited to contribute an article or articles to ram, and will receive an author's fee if your article is published.

E-mail, editor: [Martin.Stockmann@Mb.TU-Chemnitz.de](mailto:Martin.Stockmann@Mb.TU-Chemnitz.de)

E-mail, HBM: [klaus.bathe@hbm.com](mailto:klaus.bathe@hbm.com)

Reply fax to the editor: +49 (0) 371 5311471

Name \_\_\_\_\_

Company / Dept. \_\_\_\_\_

Street \_\_\_\_\_

Town, Postal code \_\_\_\_\_

Telephone \_\_\_\_\_

Fax \_\_\_\_\_

I am interested in having an article published in ram and would ask you to kindly contact me

# imprint

## Published by:

Hottinger Baldwin Messtechnik GmbH  
Im Tiefen See 45  
D-64293 Darmstadt  
Tel. +49 6151 803-0  
Fax +49 6151 803-9100  
[www.hbm.com](http://www.hbm.com)

## Editor

Dr.-Ing. habil. Martin Stockmann  
Chemnitz University of Technology

Please address any questions about ram articles to the publisher.

Please address any questions about HBM products to your local HBM sales office.

## Copyright

Copying is only permitted with the advance written approval of the editorial office or the publisher. Copying or reproduction in the form of photocopies, microfilm or other means for commercial purposes is not permitted.

## All rights reserved

No liability can be accepted for the procedures and circuits described and the names used in respect of the infringement of patents or trademarks of third parties.

## Design & Artwork

[www.contrust-design.de](http://www.contrust-design.de)

## reports in applied measurement 1/2005

Issued: June 2005

"reports in applied measurement"  
is issued twice annually

ISSN 1614-9912



measurement with confidence

**Hottinger Baldwin Messtechnik GmbH**

Im Tiefen See 45  
64293 Darmstadt  
Germany

Tel. +49 (0) 6151 803-0  
Fax +49 (0) 6151 803-9100

E-mail: [info@hbm.com](mailto:info@hbm.com)  
Internet: [www.hbm.com](http://www.hbm.com)